Int. J. Heat Mass Transfer. Vol. 17, pp. 581–593. Pergamon Press 1974. Printed in Great Britain

THREE-DIMENSIONAL COMPRESSIBLE TURBULENT BOUNDARY LAYER ON A SHARP CONE AT INCIDENCE IN SUPERSONIC FLOW

J. C. ADAMS, JR.
ARO, Inc., von Karman Gas Dynamics Facility, Arnold Engineering Development Center, Arnold Air Force Station, Tennessee, U.S.A.

(*Received* 13 *March* 1973 *and in revised form* 30 *July* 1973)

Abstract—An analytical approach toward numerical calculation of the three-dimensional turbulent boundary layer on a sharp cone at incidence under supersonic flow conditions is presented. The theoretical model is based on implicit finite-difference integration of the governing three-dimensional turbulent boundary-layer equations in conjunction with a three-dimensional scalar eddy viscosity model of turbulence. Comparison of the present theory with detailed experimental measurements of the three-dimensional turbulent boundary-layer structure (velocity and temperature profiles), as well as surface streamline direction (obtained via an oil-flow technique), reveals good agreement.

NOMENCLATURE

A_+, van Driest damping constant, 26·0;
C_p, constant pressure specific heat for air, 6006 ft^2/s^2°R;
$\bar{G}$, scalar velocity function;
h', fluctuating static enthalpy;
$\bar{h}$, mean static enthalpy;
k, laminar (molecular) thermal conductivity;
k_+, inner law mixing length constant, 0·435;
L, slant length of sharp cone;
l_+, mixing length;
M_∞, free-stream Mach number;
Pr, laminar Prandtl number for air, 0·71;
Pr_t, turbulent Prandtl number, 0·90;
$\bar{p}$, static pressure;
p_∞, free-stream static pressure;
$\dot{q}$, heat flux;
R, specific gas constant for air, 1716 ft^2/s^2°R;
$Re_{\infty,L}$, free-stream Reynolds number, $\rho_\infty U_\infty L/\mu_\infty$;
r, body radius;
$\bar{T}$, mean static temperature;
T_e, static temperature at outer edge of boundary layer;
T_0, stagnation temperature;
T_{ref}, reference temperature;
T_w, wall temperature;
T_∞, free-stream static temperature;
U_e, streamwise velocity component at outer edge of boundary layer;
U_∞, free-stream velocity;
u', fluctuating streamwise velocity component;
$\bar{u}$, mean streamwise velocity component;
V, combined normal velocity components according to equation (6);
v', fluctuating normal velocity component;
$\bar{v}$, mean normal velocity component;
W_e, crossflow velocity component at outer edge of boundary layer;
w', fluctuating crossflow velocity component;
$\bar{w}$, mean crossflow velocity component;
x, coordinate along body surface;
y, coordinate normal to body surface;
y_t, characteristic thickness of boundary layer in equation (24).

Greek letters

α, angle of attack;
γ, specific heat ratio for air, 1·40;
δ_v, sharp cone semivertex angle;
ε, eddy viscosity;
ε_i, eddy viscosity in inner region;
ε_0, eddy viscosity in outer region;
κ, eddy thermal conductivity;
λ, outer law mixing-length constant, 0·090;
μ, laminar (molecular) viscosity;
μ_∞, free-stream laminar (molecular) viscosity;
ξ, η, ζ, transformed coordinates defined by equations (28)–(30);
ρ', fluctuating mass density;
$\bar{\rho}$, mean mass density;
ρ_∞, free-stream mass density;
τ, shear stress;
τ_w, wall shear stress;
ϕ, circumferential coordinate;

ω, streamline direction, $\tan^{-1}(\bar{w}/\bar{u})$;
ω_e, streamline direction at outer edge of boundary layer, $\tan^{-1}(W_e/U_e)$;
ω_s, streamline direction at body surface, $\tan^{-1}(\tau_{w,\phi}/\tau_{w,x})$.

Subscripts

e, outer edge of boundary layer;
max, maximum value;
0, stagnation or total;
ref, reference value;
s, surface;
turb, turbulent;
w, wall;
x, x-direction;
ϕ, ϕ-direction;
∞, free-stream.

Superscripts

$'$, fluctuating quantity;
$-$, averaged quantity with respect to time.

1. INTRODUCTION

DEVELOPMENT of analysis techniques for the three-dimensional turbulent boundary layer must face the problem of how to accurately model the three-dimensional turbulent shear stress in a time-averaged Reynolds sense. The classical eddy viscosity-mixing length hypothesis by Prandtl applied to three-dimensional turbulent flows [1] suggests that the eddy viscosity should depend only on the properties of the turbulence and a local eddy scale, i.e. the eddy viscosity should be a scalar function independent of coordinate direction. Implicit in this approach is the requirement that the directions of the three-dimensional turbulent shear stress components are the same as the directions of the corresponding mean velocity gradients. As shown by Bradshaw [2] through a three-dimensional kinetic-energy-of-turbulence approach, the directions of the shear stress components are not, in general, exactly the same as the directions of the corresponding mean velocity components.

Recent analysis by Nash [3], Cooper [4], and Pierce and Klinksiek [5] concerning three-dimensional turbulent boundary layers in an incompressible flow indicate that use of the scalar eddy viscosity concept will lead to acceptable results when coupled to an accurate integration technique for numerical solution of the three-dimensional turbulent boundary-layer equations. Both Cooper and Pierce and Klinksiek applied implicit finite-difference approaches while Nash used an explicit finite-difference scheme which has recently been updated and improved [6]. The method of Nash has also been modified to include the effects of centrifugal and Coriolis forces for application to calculation of the incompressible three-dimensional turbulent boundary layer on a helicopter rotor as reported in [7]. An excellent summary of the state-of-the-art concerning three-dimensional turbulent boundary-layer analysis of incompressible fluid flow may be found in the recent book by Nash and Patel [8].

With regard to the three-dimensional compressible turbulent boundary-layer problem, little work has been done to present. The three-dimensional compressible turbulent boundary-layer equations have been derived by Braun [9] and Vaglio-Laurin [10]. Several attempts to solve these equations using integral techniques in conjunction with the so-called small crossflow assumption (which uncouples the streamwise momentum equation from the crossflow momentum equation) have been made by Cooke [11], Smith [12], and Bradley [13], as well as Braun and Vaglio-Laurin, cited previously. These integral approaches are not entirely satisfactory because of the difficulties in adequately representing the crossflow velocity profile. The analysis by Hunt, Bushnell and Beckwith [14] is the first, to the author's knowledge, to apply marching finite-difference integration to the three-dimensional compressible turbulent boundary-layer equations; this work considers hypersonic flow over a swept infinite cylinder-slab based on a scalar eddy viscosity model of three-dimensional turbulence.

The present paper reports on an analytical investigation and development of a finite-difference calculation technique for the analysis of the three-dimensional compressible turbulent boundary layer on a sharp cone at angle of attack in a supersonic flow. The sharp cone geometry at angle of attack is of obvious importance to aerodynamic and propulsion engine applications. Specifically, the governing three-dimensional turbulent boundary-layer equations for a compressible flow are simplified by the conical nature of the sharp cone flow field and numerically integrated on a digital computer utilizing a marching implicit finite-difference technique. Three-dimensional turbulence is accounted for using a three-dimensional scalar eddy viscosity approach in conjunction with an inner-outer mixing-length formalism. The inviscid conical flow field about the sharp cone at incidence is determined using a prior documented digital computer code which, in turn, furnishes the outer-edge conditions for input to the present boundary-layer analysis. To assess the accuracy and applicability of the present theory, comparisons of the calculated three-dimensional turbulent boundary-layer profiles (velocities and temperature) are made with detailed experimental flow-field surveys of the three-dimensional turbulent boundary-layer structure at various circumferential locations around a sharp cone at incidence under supersonic flow conditions.

2. ANALYTICAL ANALYSIS

Governing three-dimensional turbulent boundary-layer equations

The present analysis employs the three-dimensional compressible turbulent boundary-layer equations in terms of time-averaged mean flow quantities as derived by Vaglio-Laurin [10]. The coordinate system is taken to consist of geodesics and geodesic parallels, following Moore [15]. For the sharp cone geometry under present consideration, the geodesic coordinates are taken to be the cone generators and the geodesic parallels are the circles swept by the meridional angle. The corresponding length function $r(x)$ is the local radius of the body. See Fig. 1 for clarification of the sharp cone geometry, nomenclature, and coordinate system. The time-averaged mean velocity components

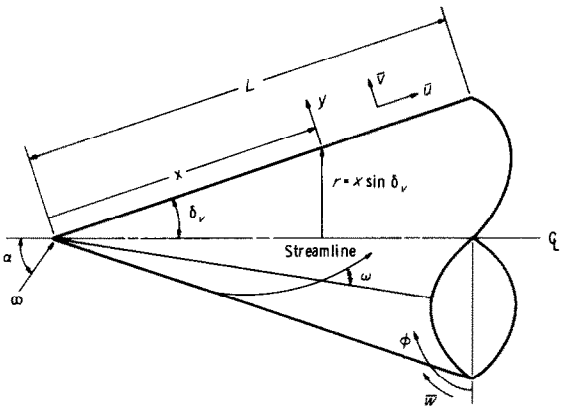

FIG. 1. Sharp cone at angle of attack geometry and nomenclature.

are taken to be $\bar{u}$, $\bar{v}$ and $\bar{w}$ in the directions of x, y and ϕ, respectively. The governing equations of motion are, following Vaglio-Laurin:

Continuity

$$\frac{\partial}{\partial x}(\bar{\rho}\bar{u}r)+\frac{\partial}{\partial y}(\bar{\rho}Vr)+\frac{\partial}{\partial \phi}(\bar{\rho}\bar{w})=0 \tag{1}$$

Streamwise (x) momentum

$$\bar{\rho}\bar{u}\frac{\partial \bar{u}}{\partial x}+\bar{\rho}V\frac{\partial \bar{u}}{\partial y}+\frac{\bar{\rho}\bar{w}}{r}\frac{\partial \bar{u}}{\partial \phi}-\frac{\bar{\rho}(\bar{w})^2}{r}\frac{\partial r}{\partial x}$$
$$=-\cancel{\frac{\partial \bar{p}}{\partial x}}^{0}+\frac{\partial}{\partial y}\left[\mu\frac{\partial \bar{u}}{\partial y}-\bar{\rho}\overline{u'v'}\right] \tag{2}$$

Circumferential (ϕ) momentum

$$\bar{\rho}\bar{u}\frac{\partial \bar{w}}{\partial x}+\bar{\rho}V\frac{\partial \bar{w}}{\partial y}+\frac{\bar{\rho}\bar{w}}{r}\frac{\partial \bar{w}}{\partial \phi}+\frac{\bar{\rho}\bar{u}\bar{w}}{r}\frac{\partial r}{\partial x}$$
$$=\frac{-1}{r}\frac{\partial \bar{p}}{\partial \phi}+\frac{\partial}{\partial y}\left[\mu\frac{\partial \bar{w}}{\partial y}-\bar{\rho}\overline{v'w'}\right] \tag{3}$$

Normal (y) momentum

$$\frac{\partial \bar{p}}{\partial y}=0 \tag{4}$$

Energy (static enthalpy)

$$\bar{\rho}\bar{u}\frac{\partial \bar{h}}{\partial x}+\bar{\rho}V\frac{\partial \bar{h}}{\partial y}+\frac{\bar{\rho}\bar{w}}{r}\frac{\partial \bar{h}}{\partial \phi}$$
$$=\bar{u}\cancel{\frac{\partial \bar{p}}{\partial x}}^{0}+\frac{\bar{w}}{r}\frac{\partial \bar{p}}{\partial \phi}+\mu\left[\left(\frac{\partial \bar{u}}{\partial y}\right)^2+\left(\frac{\partial \bar{w}}{\partial y}\right)^2\right]$$
$$-\bar{\rho}\overline{u'v'}\frac{\partial \bar{u}}{\partial y}-\bar{\rho}\overline{v'w'}\frac{\partial \bar{w}}{\partial y}+\frac{\partial}{\partial y}\left[\frac{\mu}{Pr}\frac{\partial \bar{h}}{\partial y}-\bar{\rho}\overline{v'h'}\right] \tag{5}$$

where

$$V=\bar{v}+\frac{\overline{\rho'v'}}{\bar{\rho}}. \tag{6}$$

Also implicit in the above equations is the requirement of an inviscid conical flow field which leads to the term $\partial\bar{p}/\partial x=0$; a discussion of the inviscid conical flow field about a sharp cone at incidence in a supersonic or hypersonic flow will be given later in this section.

If subscript w denotes wall and subscript e denotes outer edge of the boundary layer, the associated boundary conditions on the above defined equations are

Momentum

$$y=0:\bar{u}=\bar{v}=\bar{w}=\overline{u'v'}=\overline{v'w'}=\overline{\rho'v'}=0$$
$$\lim y\to\infty:\bar{u}\to U_e,\ \bar{w}\to W_e$$
$$\overline{u'v'}\to 0,\ \overline{v'w'}\to 0,\ \overline{\rho'v'}\to 0 \tag{7}$$

Energy

$$y=0:\bar{h}=h_w,\ \overline{v'h'}=0$$
$$\lim y\to\infty:\bar{h}\to h_e,\ \overline{v'h'}\to 0 \tag{8}$$

which reflect the requirements of no slip and no homogeneous mass injection (suction or blowing) at the wall as well as a prescribed constant wall enthalpy. The normal momentum equation (4) reveals that the static-pressure variation across the boundary layer is negligible, and hence the static pressure, $\bar{p}(\phi)$, is regarded as an external input to the boundary-layer analysis from a separate inviscid analysis. The outer-edge velocities, U_e and W_e, as well as the outer-edge static enthalpy, h_e, must be determined from the inviscid analysis consistent with the imposed static-pressure distribution.

The gas model adopted for the present study is thermally and calorically perfect air having a constant specific heat ratio $\gamma=1{\cdot}40$ and obeying the equation of state

$$\bar{p}=\bar{\rho}R\bar{T} \tag{9}$$

where $R = 1716\,\text{ft}^2/\text{s}^2{}^\circ\text{R}$. Hence, under this assumption.

$$\bar{h} = C_p \bar{T} \tag{10}$$

where $C_p = 6006\,\text{ft}^2/\text{s}^2{}^\circ\text{R}$. The laminar viscosity, μ, is taken to obey Sutherland's law

$$\frac{\mu}{\mu_{\text{ref}}} = \frac{T_{\text{ref}} + 198{\cdot}6}{\bar{T} + 198{\cdot}6}\left(\frac{\bar{T}}{T_{\text{ref}}}\right)^{3/2} \tag{11}$$

where $\bar{T}$ must have units of °R and subscript ref denotes a reference condition. The laminar Prandtl number, Pr, is taken to be a constant value of 0·71 across the entire boundary layer.

Turbulent transport laws

Before equations (1)–(3) and (5) can be solved, expressions must be supplied for the Reynolds stress or turbulent shear terms in the momentum equations and the turbulent flux of static enthalpy in the energy equation. The approach used in the present analysis is to model these terms as functions of the mean-flow variables following the analysis by Hunt, Bushnell and Beckwith [14].

The theory that the Reynolds stress in turbulent flow is proportional to a momentum exchange coefficient times the mean-flow velocity gradient normal to the surface is well known and commonly used in turbulent boundary-layer analyses. This concept is based on an assumed analogy between the so-called eddy viscosity and the molecular viscosity. The total shear components in the streamwise (x) and circumferential (ϕ) directions are written as

$$\tau_x = \mu\frac{\partial \bar{u}}{\partial y} - \bar{\rho}\overline{u'v'} = \mu\frac{\partial \bar{u}}{\partial y} + \varepsilon_x\frac{\partial \bar{u}}{\partial y} \tag{12}$$

$$\tau_\phi = \mu\frac{\partial \bar{w}}{\partial y} - \bar{\rho}\overline{v'w'} = \mu\frac{\partial \bar{w}}{\partial y} + \varepsilon_\phi\frac{\partial \bar{w}}{\partial y} \tag{13}$$

where the eddy viscosities ε_x and ε_ϕ in the x- and ϕ-directions, respectively, might in general be different. Since the total resultant shear must be a vector quantity, its magnitude is written as

$$\tau = [(\tau_x)^2 + (\tau_\phi)^2]^{1/2} = \left[(\mu+\varepsilon_x)^2\left(\frac{\partial \bar{u}}{\partial y}\right)^2 + (\mu+\varepsilon_\phi)^2\left(\frac{\partial \bar{w}}{\partial y}\right)^2\right]^{1/2}. \tag{14}$$

Applying the well-known Prandtl mixing-length hypothesis (see [1] for clarification) in conjunction with the assumption that the eddy viscosity is a *scalar* function *independent* of coordinate direction (which means physically that the turbulent shear stress acts in the mean rate of strain direction) results in an eddy viscosity relationship of the form

$$\varepsilon = \varepsilon_x = \varepsilon_\phi = \bar{\rho} l_*^2 \frac{\partial \bar{G}}{\partial y} \tag{15}$$

where $\bar{G}$ is a scalar velocity function defined by

$$\frac{\partial \bar{G}}{\partial y} = \left[\left(\frac{\partial \bar{u}}{\partial y}\right)^2 + \left(\frac{\partial \bar{w}}{\partial y}\right)^2\right]^{1/2}. \tag{16}$$

The quantity l_* is termed the mixing length and is some characteristic length related to the size or scales of eddies responsible for the flux of momentum in the y-direction. Under the above model the magnitude of the turbulent shear stress in a three-dimensional turbulent boundary layer may be written in the form

$$\tau_{\text{turb}} = \bar{\rho} l_*^2\left[\left(\frac{\partial \bar{u}}{\partial y}\right)^2 + \left(\frac{\partial \bar{w}}{\partial y}\right)^2\right]. \tag{17}$$

Hunt, Bushnell and Beckwith [14] call the above representation of the Reynolds stress the invariant turbulence model. In a recent analysis of three-dimensional incompressible turbulent boundary-layer flows using the kinetic-energy-of-turbulence approach, Nash [3] has advanced arguments that the turbulent shear stress is likely to act in the mean rate of strain direction, defined by the components of the mean velocity gradient vector, so that his closure equation is simply, in the nomenclature of the present analysis,

$$\frac{\tau_{\text{turb},x}}{\partial \bar{u}/\partial y} = \frac{\tau_{\text{turb},\phi}}{\partial \bar{w}/\partial y}. \tag{18}$$

The same equation results from the scalar eddy viscosity model presented by equation (15) above. On the other hand, Bradshaw [2] has derived a set of differential equations for the two components of the turbulent shear stress based on the kinetic-energy-of-turbulence approach but permitting the turbulent shear stress vector to deviate from the mean rate of strain direction. However, in the near-wall region, Bradshaw's turbulent shear stress equation reduces to the identical results derived above for the turbulent shear contributions. Arguments for the preference of either variance or invariance of the turbulent shear stress vector relative to the mean rate of strain direction are currently based on slender evidence.

The expression for the total heat flux in a turbulent boundary layer may be written in terms of the static enthalpy as

$$\dot{q} = \frac{k}{C_p}\frac{\partial \bar{h}}{\partial y} - \bar{\rho}\overline{v'h'} = \frac{k}{C_p}\frac{\partial \bar{h}}{\partial y} + \frac{\kappa}{C_p}\frac{\partial \bar{h}}{\partial y} \tag{19}$$

where k is the laminar (molecular) thermal conductivity and κ is the so-called eddy thermal conductivity. Using the definition of the laminar (molecular) Prandtl number

$$Pr = \frac{C_p \mu}{k} \tag{20}$$

and defining, by analogy, a turbulent Prandtl number (based on the use of static enthalpy) as

$$Pr_t = \frac{C_p \varepsilon}{\kappa} \tag{21}$$

with ε the eddy viscosity discussed previously, the total heat flux expression (19) may be written in the form

$$\dot{q} = \mu\left[\frac{1}{Pr} + \frac{\varepsilon}{\mu}\frac{1}{Pr_t}\right]\frac{\partial \bar{h}}{\partial y}. \tag{22}$$

Mixing-length model

In the manner of Escudier [16], Patankar and Spalding [17] recommend the following two-layer (inner–outer) variation of the mixing length, l_*, across the turbulent two-dimensional boundary layer which is adopted for the present three-dimensional case by noting that the scalar properties of a turbulence field are unlikely to be affected by moderate three-dimensionality because turbulence is inherently three-dimensional in nature for even so-called two-dimensional flows

$$\begin{aligned} &\text{Inner Region: } l_* = k_* y, \text{ for } 0 < y \leqslant \lambda y_l/k_* \\ &\text{Outer Region: } l_* = \lambda y_l, \text{ for } \lambda y_l/k_* < y \end{aligned} \tag{23}$$

where the values for the various numerical constants are taken to be $k_* = 0{\cdot}435$ and $\lambda = 0{\cdot}09$. The value of y at the point where the velocity in the boundary layer is equal to 0·99 of the velocity at the boundary-layer outer edge is used to define the distance y_l; i.e.

$$y_l = \left\{ y\text{-value where } \frac{[(\bar{u})^2 + (\bar{w})^2]^{1/2}}{[U_e^2 + W_e^2]^{1/2}} = 0{\cdot}99 \right\}. \tag{24}$$

The now classic analysis by van Driest [18] concluded that, in the vicinity of a wall, the turbulent contribution to the total shear stress in an incompressible two-dimensional boundary layer should be exponentially damped as the wall is approached so as to yield exactly the laminar shear stress form, $\tau = \mu(\partial \bar{u}/\partial y)$, at the wall. Following the suggestion by Patankar and Spalding [17] that, for compressible boundary-layer flows, the *local* value of shear stress be used in the van Driest exponential damping yields the following relationship for the magnitude of the three-dimensional near-wall total shear stress

$$\tau = \mu\frac{\partial \bar{G}}{\partial y} + \bar{\rho} k_*^2 y^2 \left[1 - \exp\left(\frac{-y\sqrt{\tau\bar{\rho}}}{\mu A_*}\right)\right]^2 \left(\frac{\partial \bar{G}}{\partial y}\right)^2 \tag{25}$$

where the constant A_* is taken to be 26·0 following the original van Driest proposal. Note that the damping term in equation (25) reflects the application of the *local total* shear stress as defined by equation (14).

Hence, the present analysis treats the turbulent shear stress in a three-dimensional turbulent boundary layer in terms of a two-layer inner-outer scalar eddy viscosity model. Based on equations (15), (23) and (25), the eddy viscosity expression for the inner region ($0 < y \leqslant \lambda y_l/k_*$) is

$$\varepsilon_i = \bar{\rho} k_*^2 y^2 \left[1 - \exp\left(\frac{-y\sqrt{\tau\bar{\rho}}}{\mu A_*}\right)\right]^2 \frac{\partial \bar{G}}{\partial y} \tag{26}$$

and for the outer region ($y > \lambda y_l/k_*$)

$$\varepsilon_0 = \bar{\rho}\lambda^2 y_l^2 \frac{\partial \bar{G}}{\partial y} \tag{27}$$

with the constant k_*, A_*, λ and y_l defined previously. The constraint used to define the end of the inner region and the beginning of the outer region is the continuity of the eddy viscosity. From the wall outward, the expression for the inner eddy viscosity applies until $\varepsilon_i = \varepsilon_0$, from which point the outer eddy viscosity is used.

The turbulent Prandtl number (based on the static enthalpy definition of the turbulent heat flux) as given by equation (21) is physically a measure of the ratio of the turbulent transport of momentum to the turbulent transport of heat. For the present work, the turbulent Prandtl number defined by equation (21) is taken to remain constant at the value 0·90 across the entire boundary layer as recommended by Patankar and Spalding [17] for two-dimensional turbulent boundary layers.

Procedure for numerical solution of the three-dimensional boundary-layer equations

For application in the present sharp cone at incidence investigation, the three-dimensional conical flow laminar boundary-layer analysis as presented in Appendix B of the report by McGowan and Davis [19] has been modified to include the effects of three-dimensional turbulence through the use of the scalar eddy viscosity model discussed previously. The basic McGowan and Davis laminar boundary-layer treatment is very similar to that of Dwyer [20] and Boericke [21] in that the limiting forms of the full three-dimensional compressible laminar boundary-layer equations for conical flow as originally derived by Moore [15] are solved using a marching implicit finite-difference technique for numerical integration of the nonlinear parabolic partial differential equations written in similarity variable form.

Following Appendix B of McGowan and Davis [19], the governing three-dimensional turbulent boundary-layer equations (1–5) are transformed using similarity variables ξ, η and ζ similar to those used by Dwyer [20] and Boericke [21] for three-dimensional laminar

boundary layers. The definitions of ξ, η and ζ are as follows:

$$\xi = \int_0^x r^2\,\mathrm{d}x = \int_0^x (x\sin\delta_r)^2\,\mathrm{d}x = \tfrac{1}{3}x^3\sin^2\delta_r \tag{28}$$

$$\eta = \sqrt{\frac{\rho_\infty U_\infty}{2\xi\mu_s}}\int_0^y \frac{\bar{\rho}}{\rho_s}\sqrt{\frac{\bar{p}_s}{\bar{p}}}\,r\,\mathrm{d}y \tag{29}$$

$$\zeta = \phi \tag{30}$$

where $r = x\sin\delta_r$ for the sharp cone geometry of present interest, as shown in Fig. 1. Introducing the above similarity variables into the governing equations (1)–(5) and performing the standard transformation of variables manipulations yields the set of equations (B.13)–(B.16) in Appendix B of McGowan and Davis with the following two modifications:

1. The laminar viscosity, μ, must be replaced by the sum of the laminar and turbulent (eddy) viscosity $(\mu+\varepsilon)$ in the transformed ξ- and ζ- momentum equations, as well as in the transformed energy equation. Furthermore, in the energy equation the laminar heat conductivity term (μ/Pr) must be replaced by the sum of the laminar and turbulent (eddy) heat conductivity $[(\mu/Pr)+(\varepsilon/Pr_t)]$.

2. The three-dimensional turbulent boundary-layer flow must be locally similar in the sense of a mathematical analysis under the constraint $(\partial/\partial\xi) = 0$ with the eddy viscosity ε evaluated at the *local* ξ condition. The applicability of this technique relies essentially on the condition that the external and body flow properties vary sufficiently slowly with the x-dependent variable ξ defined by equation (28). Experimental justification for the use of this assumption in the case of three-dimensional turbulent boundary-layer flow over a sharp cone at incidence in a supersonic stream is presented in Section 4 of the present paper.

Under the above local similarity restriction the transformed governing boundary-layer equations become mathematically parabolic in the η, ζ coordinates with ξ as a parameter. The "history" of the flow is contained *only* in the ε and η dependence on ζ and, hence, local similarity represents a "patching together" of *local* solutions.

The method for numerical solution of the governing three-dimensional boundary-layer equations in similarity ξ, η, ζ variables follows the iterative implicit finite-difference integration technique (integration in η-direction marching in ζ-direction windward to leeward ray) presented in Chapter III of the report by McGowan and Davis [19]. A variable η grid mesh is used to concentrate grid points in the near-wall region where the dependent variables change most rapidly in a turbulent flow. Digital computer run times are acceptable for practical usage (approximately 20 min, including printout, to integrate 180·0 degrees around a sharp cone at incidence using a 2·50-deg step size ζ-integration increment with 120 η grid points across the boundary layer on a CDC 1604-B digital computer).

Three-dimensional inviscid conical flow

The necessary outer-edge conditions for input to the above-described boundary-layer analysis are determined based on results from an inviscid analysis of a sharp cone at incidence under supersonic or hypersonic conditions following Jones [22]. Basically Jones' method uses the condition of conicity to reduce the problem to a set of elliptic nonlinear partial differential equations in two independent variables. A transformation of coordinates is used to fix the boundaries, one of which is the unknown shock wave, between which the elliptic equations are to be satisfied. The method is, in many cases, only limited by the crossflow velocity expanding from subsonic to supersonic conditions which changes the mathematical character of the governing equations from elliptic to hyperbolic, by the entropy singularity moving too far away from the surface, or by the shock approaching very close to the Mach wave. In practice these restrictions limit the allowable angle-of-attack range to $\alpha/\delta_r \lesssim 1{\cdot}4$ (see Fig. 1 for clarification of nomenclature).

The procedure for specifying the inviscid data necessary for input to the McGowan and Davis boundary-layer analysis is quite simple in that only the pressure distribution around the cone, along with the velocity and density on the windward streamline, must be specified. All other inviscid quantities are then internally calculated using the inviscid compressible Bernoulli and crossflow momentum equations applied at the cone surface, along with the restriction that the entropy remain constant on the surface, i.e. the cone surface is an isentropic surface. Complete details of this procedure are given in Section B of Chapter IV in the report by McGowan and Davis [19].

It should be pointed out that Jones [23] has recently published a very complete and thorough set of tables for inviscid supersonic and hypersonic flow about circular cones at incidence in a perfect gas, $\gamma = 1{\cdot}40$, stream. These tables can be used to provide all of the needed inviscid information for input to the present boundary-layer analysis.

3. PRIOR EXPERIMENTAL INVESTIGATIONS

The set of experimental data used for comparison with the present theory is taken from the work of Rainbird [24] concerning turbulent boundary-layer growth and separation on a yawed 12·5-deg semivertex angle sharp cone. The investigation was conducted in the Canadian National Aeronautical Establishment 5-ft intermittent blowdown (air) supersonic wind tunnel at moderate relative incidence ($\alpha/\delta_r = 1{\cdot}2$) under high

Reynolds number conditions. Reference [24] presents experimentally determined surface pressure distributions, surface flow angles, and detailed turbulent boundary-layer profile traverses at various circumferential locations around the cone.

For the present investigation, attention is restricted solely to the free-stream Mach number 1·80 and angle-of-incidence 15·78-deg condition of Rainbird [24]. The nominal free-stream conditions for this case are as follows (see Fig. 1 for the sharp cone geometry and nomenclature):

$$M_\infty = 1{\cdot}80$$
$$p_\infty = 626{\cdot}40\ \text{lbf/ft}^2$$
$$T_\infty = 321{\cdot}60°\text{R}$$
$$Re_{\infty,L} = 2{\cdot}56 \times 10^7$$
$$L = 41{\cdot}58\ \text{in.}$$

Due to the impulse nature of the blowdown tunnel flow, the cone surface temperature is taken as equal to the free-stream stagnation temperature (530°R) which results in a relatively small surface heat transfer rate from the cone to the boundary layer. Because of the conical nature of the flow field for a sharp cone at incidence (discussed in detail in Section 4 of this paper), all boundary-layer surveys at various circumferential locations around the cone were conducted at one axial location along the cone, namely, $x/L = 0{\cdot}85$. As stated by Rainbird, boundary-layer transition takes place quite close to the sharp cone apex ($x/L < 0{\cdot}1$ because of the high stream turbulence level resulting from noise generated by the blowdown wind tunnel control valve.

4. RESULTS AND DISCUSSION

Justification of locally similar turbulent boundary-layer analysis

The assumption made in Section 2 of a locally similar boundary-layer analysis with the eddy viscosity ε evaluated at the *local* ξ condition appears very questionable for application to general three-dimensional turbulent flows because of the failure to include details of the "upstream history". However, for the special case of a sharp cone at incidence in a supersonic stream where the boundary layer is in a state of fully developed turbulent flow, i.e. far downstream of transition with a constant wall temperature, experimental measurements reported by Rainbird [24] establish that the flow field, even with separation present, is essentially conical and symmetrical, thus permitting all detailed measurements to be made at one lengthwise station. The evidence in support of this finding is as follows (taken from [24]):

(a) Overall force and moment measurements show zero side force and yawing moment and give a fixed center-of-pressure position at 0·682 L that is in excellent agreement with the theoretical conical flow value of $(2/3)L/\cos\delta_v$.

(b) Integration of circumferential pressure distributions to give local normal-force coefficients shows good agreement with overall balance measurements.

(c) Measurements of surface pressure distributions along generators of the cone show pressures constant except for some extreme angle-of-attack conditions where a forward-propagating base effect is present.

(d) Flow visualization using the oil-dot technique gives values of surface flow angle ω_s, i.e. the direction of surface shear stress, as well as primary separation position which are *independent* of distance from the cone apex, x/L, within a measuring accuracy of about 1·5 deg.

Because of the importance of the invariance of the surface flow angle with lengthwise location at a given circumferential location in the present theoretical analysis, a comparison is given in Fig. 2 (taken from [24]) of surface flow angle measurements at various x/L stations up to separation for the rather severe condition of $\alpha/\delta_v = 2$. See Fig. 1 for the definition of the surface flow angle relative to the conical geometry of present interest. The results show that surface flow angle is essentially *independent* of distance from the cone apex, which means that under such a flow condition (conical inviscid and fully turbulent boundary layer) a locally similar turbulent boundary-layer analysis which neglects "upstream history" may be a plausible assumption.

A good discussion into the physical reason why a locally similar turbulent boundary layer analysis is applicable and accurate under the present flow situation may be found in the recent book by Tennekes and Lumley [25]. Under conical inviscid and fully turbulent boundary-layer conditions in regions far

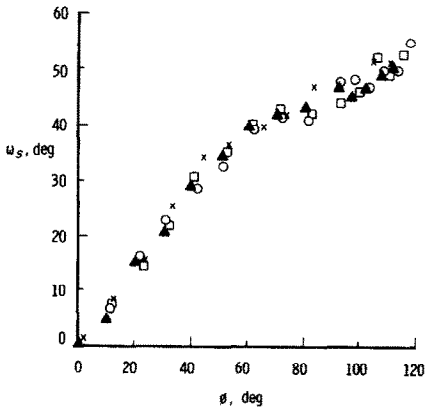

FIG. 2. Experimentally determined surface flow angles at various lengthwise stations from Rainbird [24].

removed from the sharp cone apex, the downstream changes in the flow field are simply so slow (as compared with the time scale of the turbulence) that the turbulence is in approximate equilibrium with respect to its local environment and hence "upstream history" is not important.

Presentation of present results

Turning now to representative results from the present investigation, one sees in Fig. 3 a comparison of the calculated surface pressure distribution around the sharp cone based on the Jones analysis [22, 23] relative to the experimental measurements of Rainbird [24]. As is clearly shown in Fig. 3, the agreement is excellent over the entire cone. Figure 4 presents the corresponding calculated inviscid flow parameters (streamwise and crossflow velocities, as well as static temperature) on the cone surface. These surface values are the so-called isentropic surface values discussed in Section 2.

With respect to the above, it should be noted that Rainbird [24] experimentally observed turbulent boundary-layer separation to occur at approximately 159 deg around the cone for the present flow condition and angle of incidence ($M_\infty = 1{\cdot}80$, $Re_{\infty,L} = 2{\cdot}56 \times 10^7$, $\alpha = 15{\cdot}78$ deg). As discussed by Rainbird in [24], the development of flow separation about sharp cones as the incidence angle is increased is a gradual, progressive, steady, and essentially conical process involving the formation of symmetrical lobes of vortical fluid which develop into vortices and which remain comparatively close to the cone surface on either side

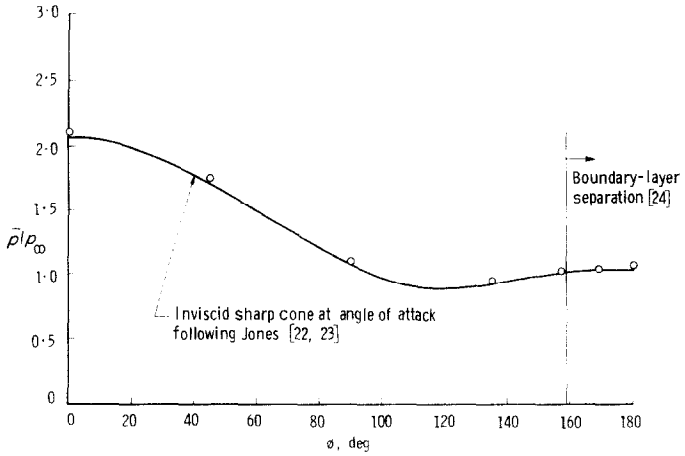

FIG. 3. Surface pressure distribution under supersonic conditions.

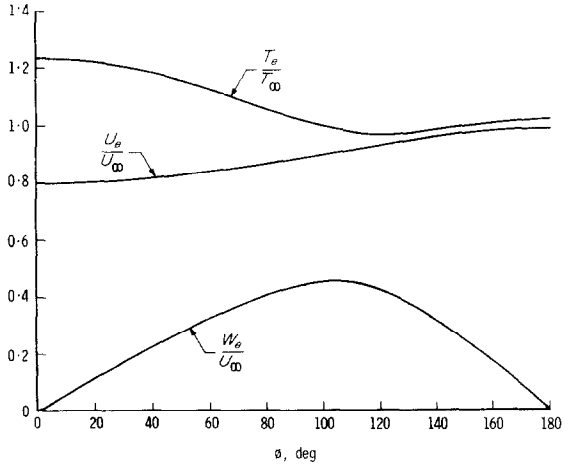

FIG. 4. Calculated inviscid flow parameters on cone surface under supersonic conditions.

of, and near, the leeward generator. For the angle of incidence of present interest ($\alpha = 15{\cdot}78$ deg) Rainbird observed the formation of two symmetrically disposed lobes of vortical fluid on either side of the leeward generator. At a higher angle of incidence ($\alpha = 22{\cdot}75$ deg) these lobes of vortical fluid roll up to form a pair of symmetrically disposed vortices close to the cone surface which, in turn, result in the formation of internal shock waves with their attendant local increases in pressure. Since there are no vortices present in the separated flow field of current interest, the influence of separation on the external inviscid flow is small, which is reflected in the excellent agreement shown in Fig. 3 between inviscid theory and experiment.

Figure 5 presents the calculated mean velocity and static temperature profiles across the turbulent boundary layer at the location $x/L = 0{\cdot}85$ on the most windward ray ($\phi = 0$ deg) of the sharp cone. The calculated profiles are generally in excellent agreement with the measured profiles by Rainbird, which reveals the validity of the presently proposed three-dimensional eddy viscosity model for windward ray applications. Also shown in Fig. 5 are comparisons of the

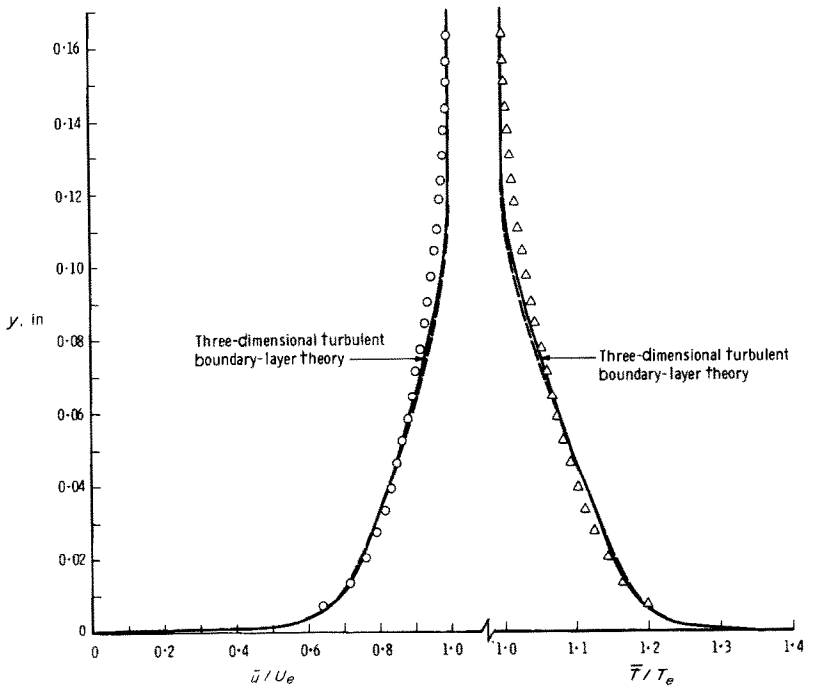

FIG. 5. Windward ray turbulent boundary-layer profiles under supersonic conditions.

present windward ray profiles relative to calculated results based upon the recent windward plane of symmetry turbulent boundary-layer analysis by Adams [26]. The basic approach of [26] involved formulation and application of a laminar, transitional, and turbulent boundary-layer analysis for the windward streamline of a sharp cone at incidence in a supersonic or hypersonic flow. The governing nonsimilar boundary-layer equations in the windward plane of symmetry were numerically integrated on a digital computer using an implicit finite-difference technique which marched along the windward ray starting at the apex of the cone with a laminar similar solution. The same two-layer (inner–outer) eddy viscosity-mixing length model of turbulence was used for calculation of the windward ray turbulent boundary layer as in the present work. The transition zone was treated through an eddy viscosity-intermittency factor approach. Inviscid edge conditions along the windward ray were obtained from the same Jones digital computer code used in the present work. The excellent agreement shown in Fig. 5 between the nonsimilar analysis of [26] and the present locally similar analysis offers further analytical justification for the applicability of the locally similar type analysis for sharp cone at incidence flows with a turbulent boundary layer.

Using the implicit finite-difference integration technique to obtain the solution around the cone at the body location $x/L = 0{\cdot}85$ yields the calculated profiles shown in Figs. 6(a)–(c) for the angular locations $\phi = 45{\cdot}0$, and 90·0, and 135·0 deg, respectively. As can be seen from these figures, agreement between the calculated profiles and the experimental profiles are in good agreement for the $\phi = 45{\cdot}0$-deg case, differ somewhat in the near-wall region for the $\phi = 90{\cdot}0$-deg case, and differ somewhat in character across the entire profile of $\phi = 135{\cdot}0$ deg. Figure 7 presents the streamline direction within the boundary layer which shows good agreement between calculated and measured values for the $\phi = 45{\cdot}0$-deg case and progressive disagreement as the ϕ-angle is increased. This behavior can be partially traced to the use of the isentropic surface values of the inviscid flow quantities as the boundary-layer outer-edge conditions. As discussed by Rainbird in the concluding paragraph of his paper, it is perhaps more appropriate to use "near" surface conditions (rather than isentropic surface conditions) as the external flow for boundary-layer calculations. The strictly correct treatment for the boundary-layer outer edge conditions requires a three-dimensional streamline-swallowing technique such as recently reported by Mayne [27].

Distributions of the surface flow angle, ω_s, and the external flow angle, ω_e, relative to experimental measurements are presented in Fig. 8. The condition that $\omega_s = 0$ on a conical surface is used as a criterion

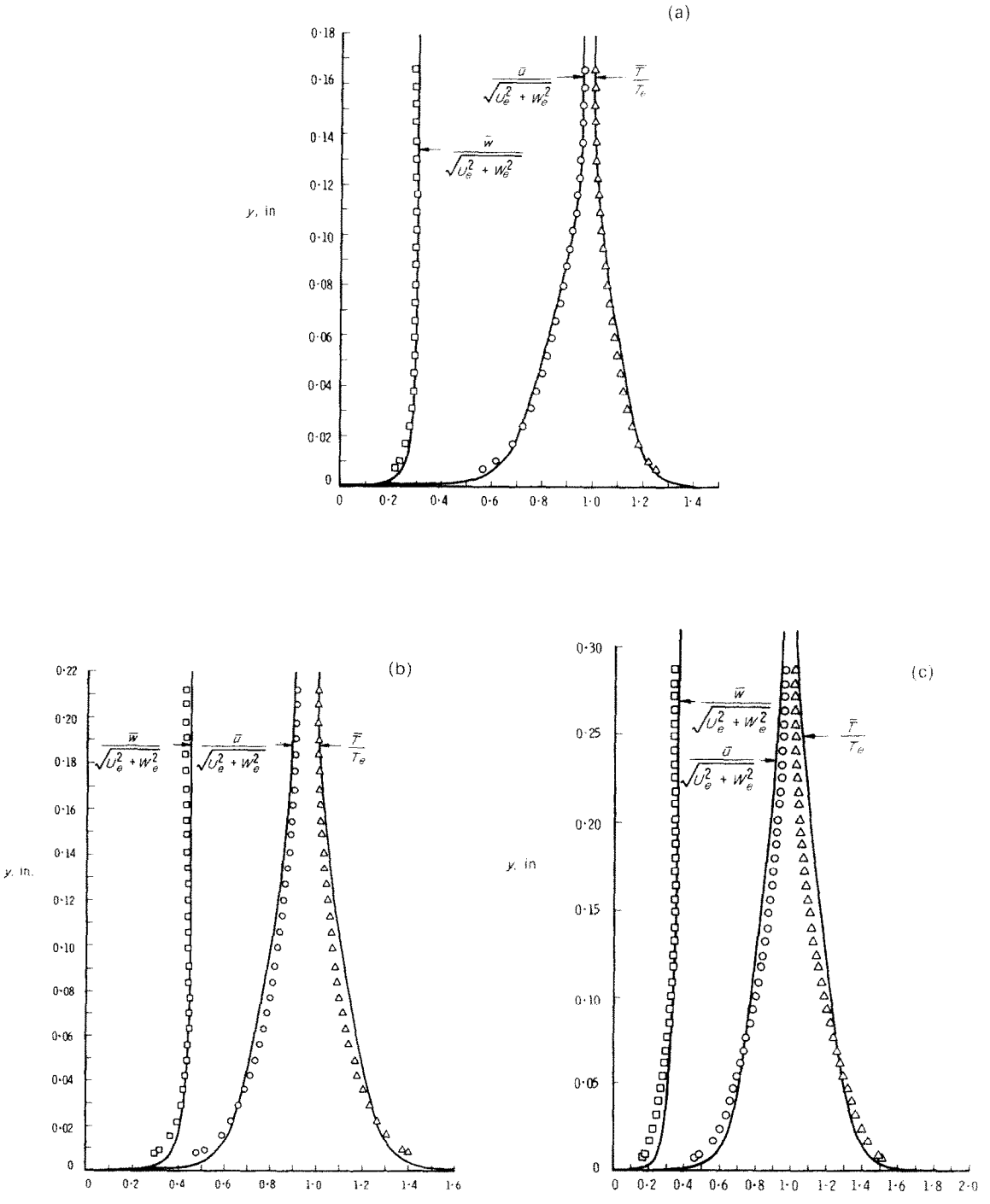

FIG. 6. Three-dimensional turbulent boundary-layer profiles under supersonic conditions. (a) $\phi = 45{\cdot}0$ deg; (b) $\phi = 90{\cdot}0$ deg; (c) $\phi = 135{\cdot}0$ deg.

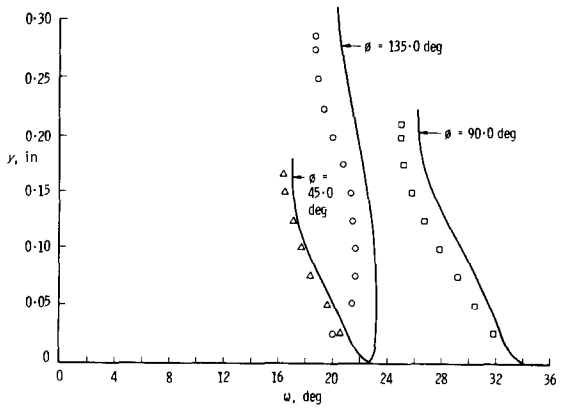

FIG. 7. Streamline directions within the three-dimensional turbulent boundary layer under supersonic conditions.

for boundary-layer separation following Rainbird. As can be seen from Fig. 8, the present three-dimensional turbulent boundary-layer analysis predicts separation to occur somewhere between $\phi = 162{\cdot}5$ and $165{\cdot}0$ deg, whereas Rainbird experimentally observed separation at $\phi \approx 159$ deg. Further note that the magnitude of the crossflow influence on the turbulent boundary-layer turning is very small, e.g. $\omega_s - \omega_e \approx 7$ deg at $\phi = 90{\cdot}0$ deg. Also shown in Fig. 8 is the calculated surface flow angle distribution for a laminar boundary layer under the same flow conditions. Much larger crossflow influence on the laminar boundary-layer turning is observed, i.e. $\omega_s - \omega_e \approx 26$ deg at $\phi = 90{\cdot}0$ deg. Laminar boundary-layer separation is predicted to occur much earlier than for the turbulent case, somewhere between $\phi = 130{\cdot}0$ and $132{\cdot}5$ deg. No attempt has been made in the present study to attempt more accurate location of the calculated separation location by use of a very small ϕ integration increment near separation; all of the present calculations employed a constant ϕ integration increment of $2{\cdot}50$ deg. In addition, accurate numerical calculation of the separation location requires treatment of viscous-inviscid interaction effects, a difficult problem not considered in the present work.

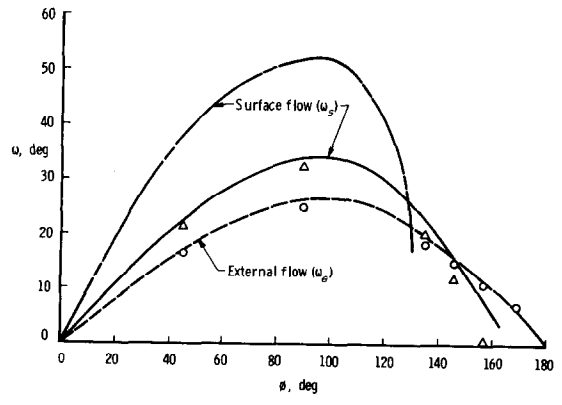

FIG. 8. Surface and external flow directions under supersonic conditions.

The calculated scalar eddy viscosity, ε, distributions across the three-dimensional turbulent boundary layer at various angular locations around the cone are presented in Fig. 9. As is apparent the eddy viscosity reaches its maximum value in the outer region of the boundary layer with $\varepsilon \gg \mu$ even in regions near the wall; e.g. $\varepsilon \approx 10\mu$ at $y \approx 0{\cdot}0025$ in. Further observe that the maximum value of the eddy viscosity increases with an increase in the ϕ angle; e.g. $\varepsilon_{max} \approx 200\mu$ at $\phi = 45{\cdot}0$ deg and $\varepsilon_{max} \approx 350\mu$ at $\phi = 135{\cdot}0$ deg. It should be noted that the laminar viscosity, μ, in the above is evaluated at the same local conditions as the corresponding eddy viscosity.

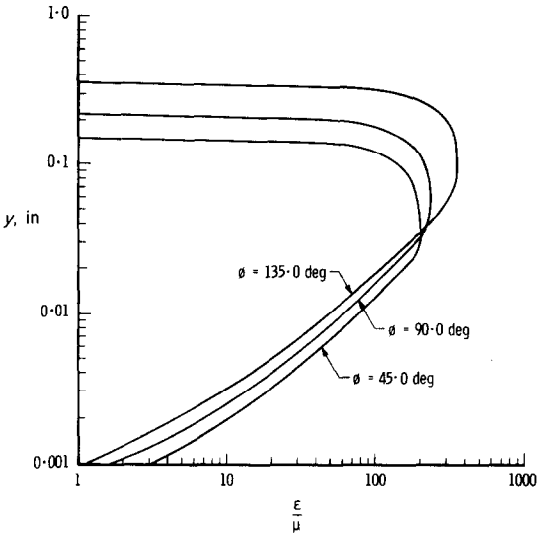

FIG. 9. Eddy viscosity distributions at various angular locations under supersonic conditions.

5. CONCLUDING SUMMARY

The above-presented results of the current investigation indicate that numerical calculation of the three-dimensional compressible turbulent boundary layer on a sharp cone at incidence in a supersonic stream is indeed feasible and reasonable, based on comparisons with experimental measurements. The assumption of a locally similar turbulent boundary-layer analysis neglecting "upstream history" appears to result in acceptable predictions of the mean flow profiles, including crossflow, when used in conjunction with a three-dimensional invariant turbulence scalar eddy viscosity model. The degree of success experienced in

the present investigation indicates that the scalar eddy viscosity approach should be applicable to numerical calculation of general three-dimensional compressible turbulent boundary-layer flows which do not separate. Application of the present method to three-dimensional turbulent boundary-layer flows on yawed sharp cones at hypersonic speeds including heat transfer effects may be found in the recent report by Adams [28].

Acknowledgements—The research reported herein was conducted by the Arnold Engineering Development Center (AEDC), Air Force Systems Command. The results were obtained by personnel of ARO, Inc., contract operator at AEDC. Further reproduction is authorized to satisfy needs of the U.S. Government.

REFERENCES

1. S. Goldstein, *Modern Developments in Fluid Dynamics*, Vol. 1, pp. 206–208. Dover, New York (1965).
2. P. Bradshaw, Calculation of three-dimensional turbulent boundary layers, *J. Fluid Mech.* **46**, 417–445 (1971).
3. J. F. Nash, The calculation of three-dimensional turbulent boundary layers in incompressible flow, *J. Fluid Mech.* **37**, 625–642 (1969).
4. P. Cooper, Turbulent boundary layer on a rotating disk calculated with an effective viscosity, *AIAA Jl* **9**, 255–261 (1971).
5. F. J. Pierce and W. F. Klinksiek, An implicit numerical solution of the turbulent three-dimensional incompressible boundary layer equations, Virginia Polytechnic Inst. and State University Rep. No. E-71-14 (1971).
6. J. F. Nash, An explicit scheme for the calculation of three-dimensional turbulent boundary layers, ASME paper 71-FE-19 (1971).
7. J. G. Hicks and J. F. Nash, The calculation of three-dimensional turbulent boundary layers on helicopter rotors, NASA CR-1845 (1971).
8. J. F. Nash and V. C. Patel, *Three-Dimensional Turbulent Boundary Layers*. Scientific and Business Consultants, Atlanta, Georgia (1972).
9. W. H. Braun, Turbulent boundary layer on a yawed cone in a supersonic stream, NASA TR R-7 (1959).
10. R. Vaglio-Laurin, Turbulent heat transfer on blunt-nosed bodies in two-dimensional and general three-dimensional hypersonic flow, *J. Aerospace Sci.* **27**, 27–36 (1960).
11. J. C. Cooke, Three-dimensional turbulent boundary layers, Aero. Res. Counc. C. P. No. 635 (1961).
12. P. D. Smith, Calculation methods for three-dimensional turbulent boundary layers, Aero. Res. Counc. R. & M. No. 3523 (1966).
13. R. G. Bradley, Approximate solutions for compressible turbulent boundary layers in three-dimensional flow, *AIAA Jl* **6**, 859–864 (1968).
14. J. L. Hunt, D. M. Bushnell, and I. E. Beckwith, The compressible turbulent boundary layer on a blunt swept slab with and without leading-edge blowing, NASA TN D-6203 (1971).
15. F. K. Moore, Three-dimensional compressible laminar boundary-layer flow, NACA TN 2279 (1951).
16. M. P. Escudier, The distribution of the mixing length in turbulent flows near walls, Imperial College, Mech. Eng. Dept. Rep. TWF/TN/1 (1965).
17. S. V. Patankar and D. B. Spalding, *Heat and Mass Transfer in Boundary Layers*. CRC Press, Cleveland, Ohio (1968).
18. E. R. van Driest, On turbulent flow near a wall, *J. Aero. Sci.* **23**, 1007–1011, 1036 (1956).
19. J. J. McGowan, III and R. T. Davis, Development of a numerical method to solve the three-dimensional compressible laminar boundary-layer equations with application to elliptical cones at angle of attack, Aerospace Research Labs. Rep. No. 70-0341 (1970).
20. H. A. Dwyer, Boundary layer on a hypersonic sharp cone at small angle of attack, *AIAA Jl* **9**, 277–284 (1971).
21. R. R. Boericke, Laminar boundary layer on a cone at incidence in supersonic flow, *AIAA Jl* **9**, 462–468 (1971).
22. D. J. Jones, Numerical solutions of the flow field for conical bodies in a supersonic stream, *C.A.S.I. Trans.* **3**, 62–71 (1970).
23. D. J. Jones, Tables of inviscid supersonic flow about circular cones at incidence $\gamma = 1{\cdot}4$, Parts I and II, AGARDograph 137 (1969).
24. W. J. Rainbird, Turbulent boundary-layer growth and separation on a yawed cone, *AIAA Jl* **6**, 2410–2416 (1968).
25. H. Tennekes and J. L. Lumley, *A First Course in Turbulence*, pp. 49–50. The MIT Press, Cambridge, Mass. (1972).
26. J. C. Adams, Jr., Implicit finite-difference analysis of compressible laminar, transitional, and turbulent boundary layers along the windward streamline of a sharp cone at incidence, Arnold Engineering Development Center TR-71-235 (AD734535) (1971).
27. A. W. Mayne, Jr., Analysis of laminar boundary layers on right circular cones at angle of attack, including streamline-swallowing effects, Arnold Engineering Development Center TR-72-134 (AD750130) (1972).
28. J. C. Adams, Jr., Analysis of the three-dimensional compressible turbulent boundary layer on a sharp cone at incidence in supersonic and hypersonic flow, Arnold Engineering Development Center TR-72-66 (AD743003) (1972).

COUCHE LIMITE TURBULENTE TRIDIMENSIONNELLE ET COMPRESSIBLE SUR UN CONE EFFILE EN INCIDENCE DANS UN ECOULEMENT SUPERSONIQUE

Résumé—On présente le calcul numérique de la couche limite turbulente et tridimensionnelle sur un cône effilé, en incidence dans un écoulement supersonique. Le modèle théorique est basé sur l'intégration, par la méthode des différences finies, des équations de la couche limite turbulente. On utilise un modèle de turbulence tridimensionnelle qui introduit une viscosité turbulente scalaire. Une comparaison de cette théorie avec des mesures sur la structure tridimensionnelle de la couche limite (profils de vitesse et de température) et sur la direction des lignes de courant (obtenue par une technique d'écoulement d'huile), révèle un bon accord.

DREIDIMENSIONALE KOMPRESSIBLE TURBULENTE GRENZSCHICHT AN EINEM SCHARFEN EINLAUFKEGEL IN ÜBERSCHALLSTÖMUNG

Zusammenfassung—Es wird eine analytische Methode der numerischen Berechnung einer dreidimensionalen turbulenten Genzschicht an einem scharfen Einlaufkegel unter supersonischen Strömungsbedingungen angegeben. Das theoretische Modell beruht auf einer impliziten Integration endlicher Differenzen der maßgebenden Gleichungen für die dreidimensionale turbulente Grenzschicht in Verbindung mit einem dreidimensionalen skalaren Scheinreibungsmodell für Turbulenz. Der Vergleich der angegebenen Theorie mit ausführlichen Messungen der dreidimensionalen turbulenten Grenzschichtstruktur (Geschwindigkeits-und Temperaturprofile) sowie der Richtung der Stromlinien an der Oberfläche (gewonnen durch Anwendung einer Oelstromtechnik) zeigt gute Übereinstimmung.

ТРЕХМЕРНЫЙ СЖИМАЕМЫЙ ТУРБУЛЕНТНЫЙ ПОГРАНИЧНЫЙ СЛОЙ НА ОСТРОМ КОНУСЕ С УГЛОМ АТАКИ В СВЕРХЗВУКОВОМ ПОТОКЕ

Аннотация — Даётся аналитический подход, сводящийся к численному расчёту трёхмерного турбулентного пограничного слоя на остром конусе с углом атаки в условиях сверхзвукового течения. Теоретическая модель основана на неявной конечно-разностной схеме численного интегрирования осредненных уравнений трехмерного турбулентного пограничного слоя при принятии трехмерной скалярной модели турбулентности для вихревой вязкости. Обнаружено хорошее соответствие между настоящей теорией и подробными экспериментальными данными о структуре трехмерного турбулентного пограничного слоя (профили скорости и температуры), а также о картине поверхностных линий тока, полученных с помощью метода масляных плёнок.